Article

Comparison of Offline, Real-Time Models and Hardware-in-the-Loop Test Results of a Power Take-Off for Wave Energy Applications

Luca Castellini [1]**, Federico Gallorini** [2]**, Giacomo Alessandri** [2]**, Erick Fernando Alves** [3]🆔**, Dan Montoya** [3]**, Bhavana Mudigonda** [3,4],*🆔 **and Elisabetta Tedeschi** [3,4],*🆔

1   UMBRAGROUP s.p.a, 06034 Foligno, Italy
2   VGA S.R.L., 06053 Deruta, Italy
3   Department of Electric Power Engineering, Norwegian University of Science and Technology (NTNU), 7034 Trondheim, Norway
4   Department of Industrial Engineering, University of Trento, 38123 Trento, Italy
*   Correspondence: bhavana.mudigonda@ntnu.no (B.M.); elisabetta.tedeschi@ntnu.no (E.T.)

Abstract: The power take-off (PTO) of a wave energy converter (WEC) converts mechanical power extracted from the waves into electrical power. Increasing PTO performance under several operational conditions is therefore essential to reduce the levelized cost of energy of a given wave energy concept and to achieve higher levels of technology readiness. A key task in the WEC design will then be the holistic assessment of the PTO performance in combination with other subsystems. It is hence important that WEC designers are aware of the different modeling options. This paper addresses this need and presents two alternative wave-to-wire modeling approaches based on a 250 kW modular electromechanical PTO coupled to an oscillating wave surge converter (OWSC) device. The first is a detailed and accurate offline model. The second model is a simplified and faster version of the first, being adequate for rapid analyses and real-time (RT) simulation. The paper presents the benchmarking of the offline model against the RT model and the hardware-in-the-loop (HIL) tests of the PTO. The normalized root-mean-square error (NRMSE) is considered as a quantitative indicator for the measurement of real-time and HIL test results against the offline simulation. Results show that the dynamics of the offline model are well represented by the RT model with execution times up to 10 times faster. The offline model also depicts well the behavior observed in the HIL tests with the NRMSE values for the PTO position, velocity, and force above 0.90, which shows the HIL test results replicates with fidelity the dynamic behavior of the complete model. Meaningful differences are however present and highlighted in this paper. An understanding of the advantages and drawbacks of these three approaches is fundamental to properly design a WEC during its project cycle and validate PTO concepts with a certain level of simplification.

Keywords: wave energy conversion; systems modeling; power take-off; ballscrew; electric generator; test bench

1. Introduction

There is a renewed urge for innovative and efficient ways of converting, transmitting and storing energy as the world transitions to carbon neutral and sustainable energy systems. The European Union has set ambitious goals towards carbon neutrality by 2050 [1] and ocean energy can play a crucial role to reach those, having a declared target of 40 GW of installed power by 2050 [2].

Wave energy has, on one hand, a tremendous potential at a global level and is one of the most promising forms of ocean energy. Developing a WEC is, on the other hand, still a complex and evolving subject. Aspects that prevented wave energy to reach a technical and commercial maturity comparable to other renewable energy technologies include

the abundance of substantially different design concepts, the variability of input loads, the harsh marine environment, and high installation and maintenance costs [3–5].

PTOs are of primary significance among the subsystems in a WEC. They are critical to define aspects such as reliability, survivability, controllability, and maintainability and have a direct impact on the energy yield of the overall device [3–5]. Moreover, the PTO may account for up to 22% of the costs in a typical wave energy project [6].

A modular PTO system has been recently developed by UMBRAGROUP based on a novel electrical machine that converts slow-speed, reciprocating linear motion into electric power with a high efficiency and reliability [7,8]. The modular nature of this PTO system was also explored during the selection and early design phases of a WEC [9,10] under the Innovative Method for Affordable Generation IN ocean Energy (IMAGINE) project within the European Union's Horizon 2020 research and innovation program.

Testing and integration with other subsystems should however be pursued from an early design phase considering how important the PTO is in a WEC. These tasks are typically achieved through a simulation of wave-to-wire models [11]. Wave-to-wire models that model the energy conversion chain from wave to grid help understanding the system dynamics and its overall response for various sea states. The accuracy [12] and computational speed [13] of the model is critical when developing control algorithms targeting the improved efficiency of a PTO. There is also a need for wave-to-wire models' fidelity and low computational requirements in the early stages of WEC development for component selection [14] and site assessment.

Moreover, the HIL testing scheme is considered as a state-of-the-art tool to validate models and bridge the gap between the laboratory and the real operational environment in several industries, such as automotive, aerospace, and power systems. HIL testing has already been used in the wave energy sector for different PTO concepts [15–20].

Two alternative wave-to-wire modeling approaches were presented in [21] to assess the expected performance of a WEC employing UMBRAGROUP's PTO system. The first was an offline model including an OWSC device, a modular PTO system based on a parallel electromechanical unit (EMU), power converters, and all controllers and functionalities required to operate a WEC safely, reliably, and efficiently. The second model was a simplified and faster version of the first, which was suitable for RT HIL testing. The performances of these two models were compared using the NRMSE as a quantitative metric.

This paper extends and further analyzes the two mentioned wave-to-wire approaches introduced in [21] and compares their performance against a HIL test setup of UMBRA-GROUP's PTO system. The main goals of this work were to: (1) describe these two wave-to-wire models and the HIL test setup; (2) compare the offline model to the RT model and the HIL tests; and (3) emphasize the advantages and drawbacks of each model, highlighting for which purposes they are adequate during the WEC project cycle.

2. Background

The aim of the IMAGINE project was designing, manufacturing, and testing a novel linear generator to decrease the cost of current PTO technologies, while increasing their efficiency and reliability. A ballscrew in association with an electromechanical generator (EMG) was the core element of the PTO in the proposed concept. Ballscrews are load-carrying mechanical components where the balls convert the slow-speed linear motion of the input shaft into a high-speed rotary motion of the nut and vice-versa. They have typically high efficiencies due to the low rolling friction between balls and threads. Moreover, permanent magnets integrated in the nut produce a magnetic rotating field coupled to an externally mounted stator. The screw pitch (i.e., the axial distance between adjacent threads) and the number of poles of the rotor act, respectively, as mechanical and magnetic gears, increasing the frequency of the induced voltage.

In the context of the IMAGINE project, the target of designing a 250 kW modular EMG started by identifying the loading envelope that the generator would have been

subject to. Three different WEC types and three deployment sites were evaluated in this task [9]. The selection process concluded with the identification of the OWSC concept as the preferred reference device for the estimation of the detailed EMG input data. The choice was primarily related to the capability of this architecture to constrain the stroke under different working conditions. A scaling exercise was conducted to have a WEC hosting a PTO system consisting of four 250 kW peak power EMGs in parallel given the available energy at the selected deployment sites. The deployment of modular units was then performed; each EMG would be composed of two 125 kW EMUs working in unison. This arrangement was selected to provide redundancy and to demonstrate the capability of the modular EMG to work in parallel. Figure 1 provides an overview of the EMG along the WEC width and of the kinematics linking the EMG and the OWSC flap.
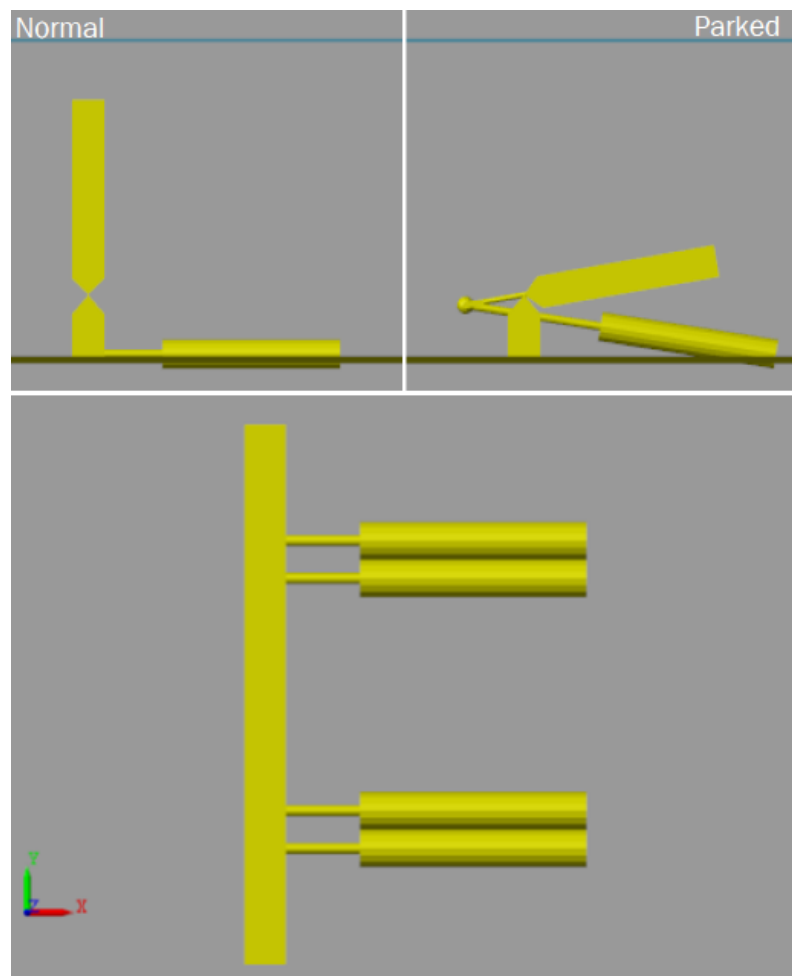

Figure 1. Views with rest and extended PTO conditions of the IMAGINE OWSC model (IMAGINE project, 2018).

Generic load cases were analyzed to identify the overall EMG's loading envelope. Those included power production, occurrence of faults, start-up, and parking in several relevant sea states. Force and power limits were then integrated to allow the EMG working within its operative conditions, 165 kN and 250 kW, respectively, with a maximum achievable EMG speed of 1500 rpm. The power limit was a constraint of the IMAGINE project, while the force limit was set according to a preliminary design of the ballscrew. The PTO damping was identified in an optimization procedure starting from a pure passive control law to maximize the mean annual energy production for each relevant sea state. From the optimal damping the optimization algorithm then tried to tune the PTO stiffness or inertia to achieve an optimal reactive control law aiming to increase the energy production

even further. The maximum values of relevant variables were extracted from the numerical simulation results to define the overall loading envelope.

Taking these into account, the final EMG design contained two EMUs with moving ball nuts and rotating screws, connected to the same moving flange. The screw was connected to the rotor of a permanent magnet synchronous machine (PMSM) at one end, while a support with a roller bearing withstood the screw weight and allowed its rotation on the other end. Figure 2 provides an overview of the EMG's main components.
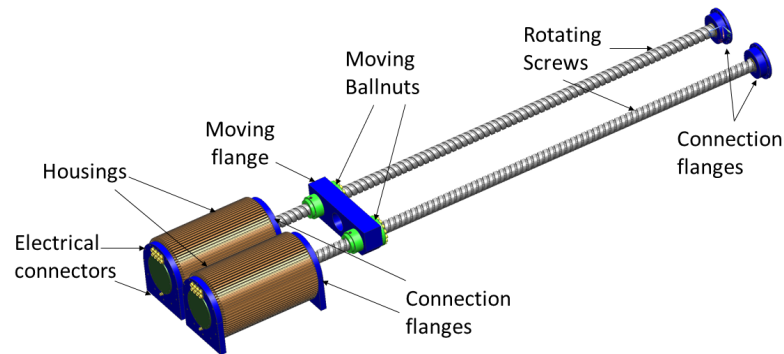

Figure 2. EMG design (IMAGINE project, 2019).

A test rig was designed by VGA according to the proposed PTO concept by connecting an EMG and an EMU to the same carriage. This approach allowed the testing of the EMG both as a generator and an actuator, thanks to the reversibility of the ballscrew and PMSM technologies. The EMU could exert a load when the EMG was used as a generator. Tests under this configuration allowed the demonstration of the EMG's modularity when employing EMUs in parallel. The EMU could be tested up to its maximum operating limits when the EMG worked as an actuator. This configuration was used to demonstrate the coherence with the input design data. Figure 3 provides an overview of the test-rig layout, while Figure 4 depicts the EMU installed in the HIL test rig.
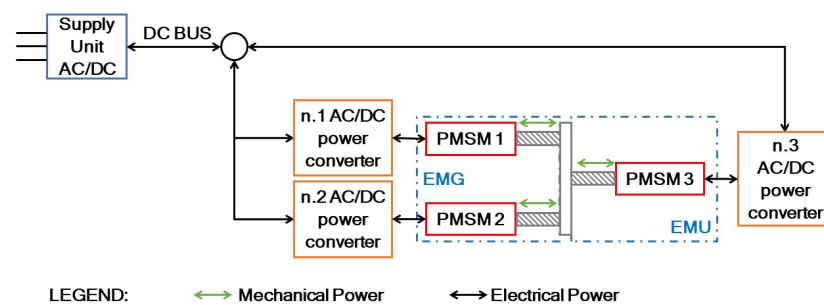

Figure 3. IMAGINE's test rig layout (IMAGINE project, 2020).

Figure 4. EMU installed on the HIL test rig at VGA facilities.

3. Offline Model

The PTO performance was evaluated by a detailed wave-to-wire model developed by NTNU and integrating the following subsystems: the OWSC device, the PTO system based on parallel EMUs, the power converters, the controllers, and electrical components. The simulation model, shown in Figure 5, was developed in Matlab/Simulink v2018a using the WEC-Sim [22] toolbox v3.0 and the Simscape Power Systems 6.9 library.
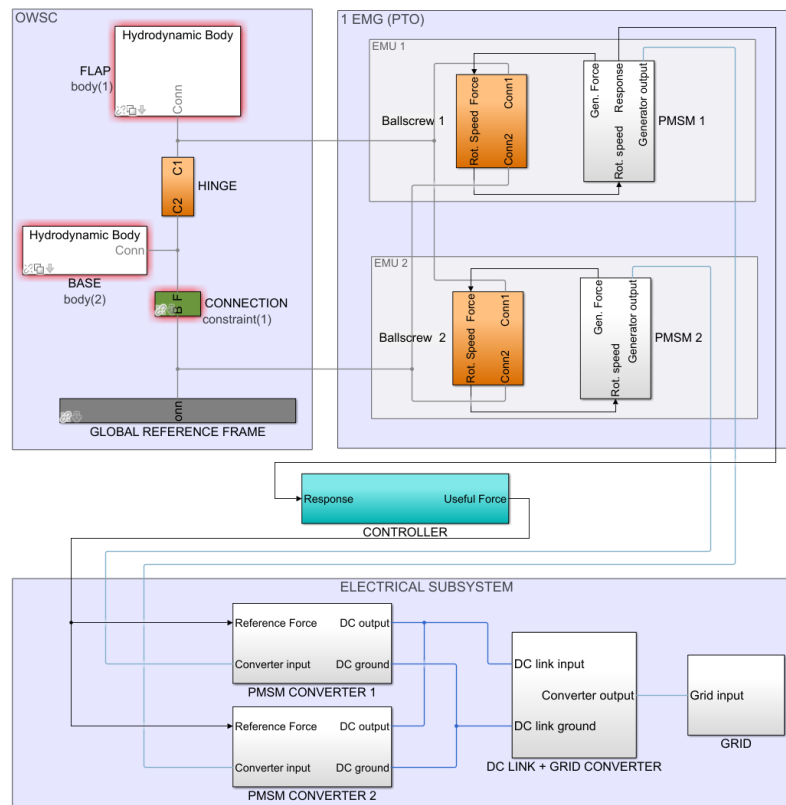
Figure 5. Offline Matlab/Simulink Model including the WEC, PTO, and control and electrical subsystems.

The hydrodynamic model of the OWSC's WEC is formed by the *FLAP*, *HINGE*, *BASE*, *fixed CONNECTION*, and *seabed* blocks. The EMG (Figure 2) is formed by two EMUs, each composed of a ballscrew and a PMSM. In the corresponding model, (Figure 5), the input to each *Ballscrew* block is the applied force originated in the PMSM, while its output is the angular speed of the PMSM.

The *PMSM* block models the electrical generator, its input being the angular speed from the ballscrew and its output the PMSM's force, further connected to the *Ballscrew* block. An additional port, containing the PMSM's stator variables, is connected to the *PMSM converter* block, composed of the average model of a 2-level, three-phase voltage source converter (VSC) using sinusoidal pulse width modulation (SPWM). The two *PMSM CONVERTER* blocks share the same dc link (input port), while their three-phase (output) port is linked to the *PMSM* blocks. The reference signal to control the converter comes from the *CONTROLLER* block, which is further explained later in this section. Finally, the *DC LINK + GRID-SIDE CONVERTER* block models the grid-side converter. As for the PMSM converter, this is also the average model of a 2-level, three-phase VSC applying SPWM. It has two input/output ports: the dc link port and the connection to the grid, respectively. The *GRID* block includes a transformer and an infinite bus.

The *CONTROLLER* block is a high-level controller that implements the previously described control optimization strategy, which selects between a passive and reactive control law to maximize power production according to the sea state. The controller sends each EMU a reference force signal, which is then converted into a PMSM's reference torque (current) on each *PMSM CONVERTER* block. In turn, in order to set the optimum EMU's reference force, the controller considers the signals provided by the EMG, namely, the PTO position, speed, and acceleration.

Table 1 presents a summary of the main parameters of the offline model. For the rest of this paper, the variables $\psi_{pm}, I_s^*, i_d^*, i_q^*, I_{max}, V_{max}, L_d, L_q, \omega_e$, and p refer to the permanent magnet flux linkage, stator total current, d- and q-axis reference currents, stator maximum current and voltage, total inductance in the d- and q-axis, electrical angular speed, and number of pole pairs of the PMSM.

Table 1. Parameters of the offline model blocks.

Flap		
Width 14.3 m	Thickness 1.1 m	Height 6.6 m
Base		
Width 14.3 m	Thickness 1.1 m	Height 2.2 m
Seabed	**Hinge**	**Ballscrew**
Water depth 10.8 m	Height from seabed 2.2 m	Pitch 60 mm
PMSM		
V_{max} 690 V_{rms}	p 20 pairs	ψ_{pm} 0.235 Wb
I_{max} 185.2 A_{rms}	L_d 1.003 mH	L_q 1.203 mH
Generator Converter		
V_{ac} 690 V_{rms}	2-level VSC with SPWM	V_{dc} 1000 V
Grid Converter		
V_{ac} 400 V_{rms}	2-level VSC with SPWM	V_{dc} 1000 V
DC Link	**Grid**	
Capacit. 100 mF	Series induct. 0.102 mH	Freq. 50 Hz

MTPA and FW

The PTO reference force is converted into a PMSM reference torque (T^*), which is then transformed into I_s^* inside each generator's power converter block. A low-level controller adjusts this reference to comply with the I_{max} and V_{max} constraints applying both maximum torque per ampere (MTPA) and field-weakening (FW) techniques [23,24]. The nonlinear equation system formed by Equations (1)–(3) is solved to set i_d^*, i_q^* using MTPA. The FW

technique readjusts i_q^* to satisfy the V_{max} limit of the PMSM solving the fourth degree polynomial seen in Equation (4) [25].

$$T^* = \frac{3}{2}p(\psi_{pm}i_q^* + (L_d - L_q)i_q^*i_d^*) \tag{1}$$

$$i_d^* = \frac{\psi_{pm} - \sqrt{\psi_{pm}^2 + 8(L_q - L_d)^2 I_s^{*2}}}{4(L_q - L_d)} \tag{2}$$

$$i_q^* = sign(I_s^*)\sqrt{I_s^{*2} - i_d^{*2}} \tag{3}$$

$$A_4 i_q^{*4} + A_3 i_q^{*3} + A_2 i_q^{*2} + A_1 i_q^* + A_0 = 0 \tag{4}$$

where

$$A_4 = 9p^2(L_d - L_q)^2 L_q^2 \omega_e^2 \tag{5}$$

$$A_3 = 0 \tag{6}$$

$$A_2 = 9p^2\psi_{pm}^2 L_q^2 \omega_e^2 - 9p^2(L_d - L_q)^2 V_{max}^2 \tag{7}$$

$$A_1 = -12T^* p\psi_{pm}L_d L_q \omega_e^2 \tag{8}$$

$$A_0 = 4T^{*2} L_d^2 \psi_{pm}^2 \tag{9}$$

The readjusted value of i_d^* given by the FW algorithm is obtained using Equation (10).

$$i_d^* = -\frac{\psi_{pm}}{L_d} + \frac{1}{L_d}\sqrt{\left(\frac{V_{max}}{\omega_e}\right)^2 - L_q^2 i_q^{*2}} \tag{10}$$

4. Pretest Real-Time Model

The RT model was developed by NTNU and VGA from the offline version presented in Section 3 to: (1) check the feasibility of running the offline model in a RT HIL platform; (2) be integrated in the test rig described in Section 2 for the EMG's qualification tests under the IMAGINE project. The model included two subsystems: (1) *SC_GUI*, integrating all elements required for the supervision and control of the test rig; (2) *SM_PLANT* (Figure 6), including all the dynamic models required for the RT simulation.
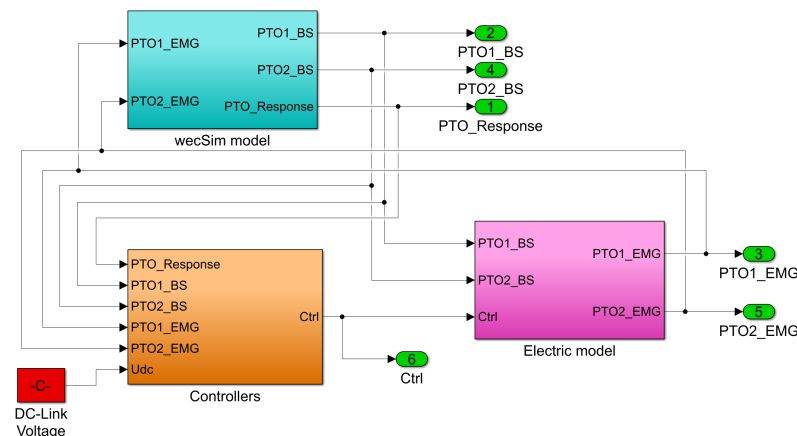

Figure 6. Components of the *SM_PLANT* subsystem.

The *wecSim model* block integrates the OWSC model and the kinematics of the PTO. It receives the torque applied by each EMU and calculates the equilibrium between PTOs and hydrodynamic loads defining the position, speed, and acceleration at the EMG's axis.

The *Controllers* block is organized in two different levels. First, a high-level controller that implements an adaptive PTO control strategy defines the reference torque that the

EMU should apply to produce a certain force at the input axis and maximize the WEC power extraction. Then, a low-level controller defines the three-phase voltage to be applied at the PMSM for achieving the reference torque.

The *Electric model* block simulates the PMSM's dynamics that, according to the input three-phase voltages and EMG's rotor speed, defines the corresponding currents and thus the output torque exerted by each EMU.

To implement FW and MTPA concurrently in the *Controllers* block as described in Section 3, it is necessary to solve a nonlinear system of equations and a fourth degree polynomial for every simulation step. This task demands a reasonable amount of processing power and it is not suitable for real-time embedded systems. Therefore, a near-optimal implementation of the FW and MTPA problems was developed to achieve RT performance. This solution is inspired by [24,26] and presented in the following algorithm:

$$i_{d,MTPA} = \frac{\psi_{pm} - \sqrt{\psi_{pm}^2 + 8(L_q - L_d)^2 I_s^{*2}}}{4(L_q - L_d)}$$

$$i_{d,MTPA} = max(i_{d,MTPA}; -I_{max})$$

$$i_{q,MTPA} = sign(I_s)\sqrt{I_s^{*2} - i_{d,MTPA}^2}$$

$$\omega_{base} = \frac{V_{max}}{\sqrt{(L_d i_{d,MTPA} + \psi_{pm})^2 + (L_q i_{q,MTPA})}}$$

IF $|\omega_e| \leq \omega_{base}$

$\quad i_d^* = i_{d,MTPA}$

$\quad i_q^* = i_{q,MTPA}$

ELSE

$$aux = (L_d^2 - L_q^2)(\psi_{pm}^2 + (L_q I_s^*)^2 - (\frac{V_{max}}{\omega_e})^2)$$

$$i_{d,FW} = \frac{-\psi_{pm}L_d - \sqrt{(\psi_{pm}L_d)^2 - aux}}{(L_d^2 - L_q^2)}$$

$$i_d^* = max(i_{d,MTPA}; -I_{max})$$

$$i_q^* = \sqrt{I_s^{*2} - (i_d^*)^2}$$

$$T_{FW} = \frac{3}{2}p i_q^*(\psi_{pm} + (L_d - L_q)i_d^*)$$

IF $T_{FW} \geq T^*$

$$i_q^* = \frac{T^*}{T_{FW}}i_q^*$$

ENDIF

ENDIF

5. Case Study with Pretest Real-Time Model

To compare the fidelity of the pretest RT and offline models, the WEC was simulated in several operational conditions for a total of 900 s. Table 2 presents results for two representative sea states of a target site off the south-west coast of England (coordinates 49.8 N 5.8 W). These are the sea states with the highest mean annual energy production ($T_p = 7$ s, $H_s = 2.25$ m) and forces ($T_p = 8$ s, $H_s = 5.25$ m).

Table 2. NRMSE-based quantitative comparison between offline and real-time models.

Variable	$T_p = 7\,s$ $H_s = 2.25\,m$	$T_p = 8\,s$ $H_s = 5.25\,m$
PTO position	0.976	0.998
PTO velocity	0.982	0.998
PTO acceleration	0.968	0.996
PTO force	*0.873*	0.971
EMG's measured torque	*0.859*	0.967
EMG's reference torque	*0.848*	0.988
EMG's mechanical power	0.965	0.920
EMG's electrical power	0.945	0.901

The NRMSE was used as a metric to quantitatively compare the models:

$$NRMSE(x_{RT}, x_{off}) = 1 - \sqrt{\frac{\sum_{n=1}^{N}(x_{RT} - x_{off})^2}{\bar{x}_{off}}} \tag{11}$$

where N is the number of samples for the entire simulation and x_{RT}, x_{off} are the values of the pretest RT and offline models, respectively. The proposed metric compares two models without accounting for the error sign and is a measure of accuracy [27]. Its values vary between $-\infty$ (bad fit) and 1 (perfect fit).

The results from Table 2 reveal that the pretest RT model could reproduce the dynamics of the offline model with fidelity. However, discrepancies on the force, reference and output torque were present. When investigating the results closer, two main sources of deviations were found: (1) the discretization of control loops in the RT model; (2) the different field-weakening strategies in the two models.

The first source caused an overshoot of the current controllers due to the additional delay introduced by the discretization of integrators. This effect is well-documented in the control systems literature, such as in [28], and better visualized in Figure 7a. The overshoot was more prominent in sea states with a lower H_s because the EMG's current and torque controllers operated without saturation for longer periods. As consequence, the NRMSE values of the PTO force, the EMG measured, and reference torques were reduced in these sea states. To achieve the offline model performance, the current controllers in the RT model should be retuned considering the delays introduced by the discretization. For a HIL setup, measurement and communication delays must also be considered.

The second source of discrepancy is better visualized in Figure 7b. In sea states with a higher H_s, the velocity often went above the EMG's rated speed, and hence the FW algorithm was activated more frequently. By comparing the EMG's current behavior between the models, one notices that the reduction of the absolute value of i_q and the increase of i_d during FW was sharper in the RT model. This happened because the RT implementation was near-optimal and prioritized keeping voltage and current limits of the PMSM within allowed limits.

All in all, the pretest RT model was regarded as a valuable tool for the EMG's qualification tests of IMAGINE. It allowed the testing of the modular PTO system developed by UMBRAGROUP in very realistic simulation conditions but under the RT constraints of VGA's HIL test rig.

Not least, the RT model could be used for other purposes in a WEC design cycle using UMBRAGROUP's modular PTO concept. For instance, a better evaluation of a WEC performance was achieved when specifying physical constraints for each component [11]. The RT model's faster performance (up to 10 times faster than the offline model) may allow the inclusion of these constraints in the initial assessment of a target site where several sea states must be simulated to evaluate important design variables such as the energy yield, peak stroke, velocity, acceleration, forces, and power.

On the other hand, it is important to keep in mind the pretest RT model's limitations. The peak PTO force may be slightly overestimated in sea states with a lower H_s, while the average power may be slightly underestimated in sea states with a higher H_s. For a detailed evaluation of a specific sea state, including the WEC performance during faults, the use of the offline model is highly recommended.
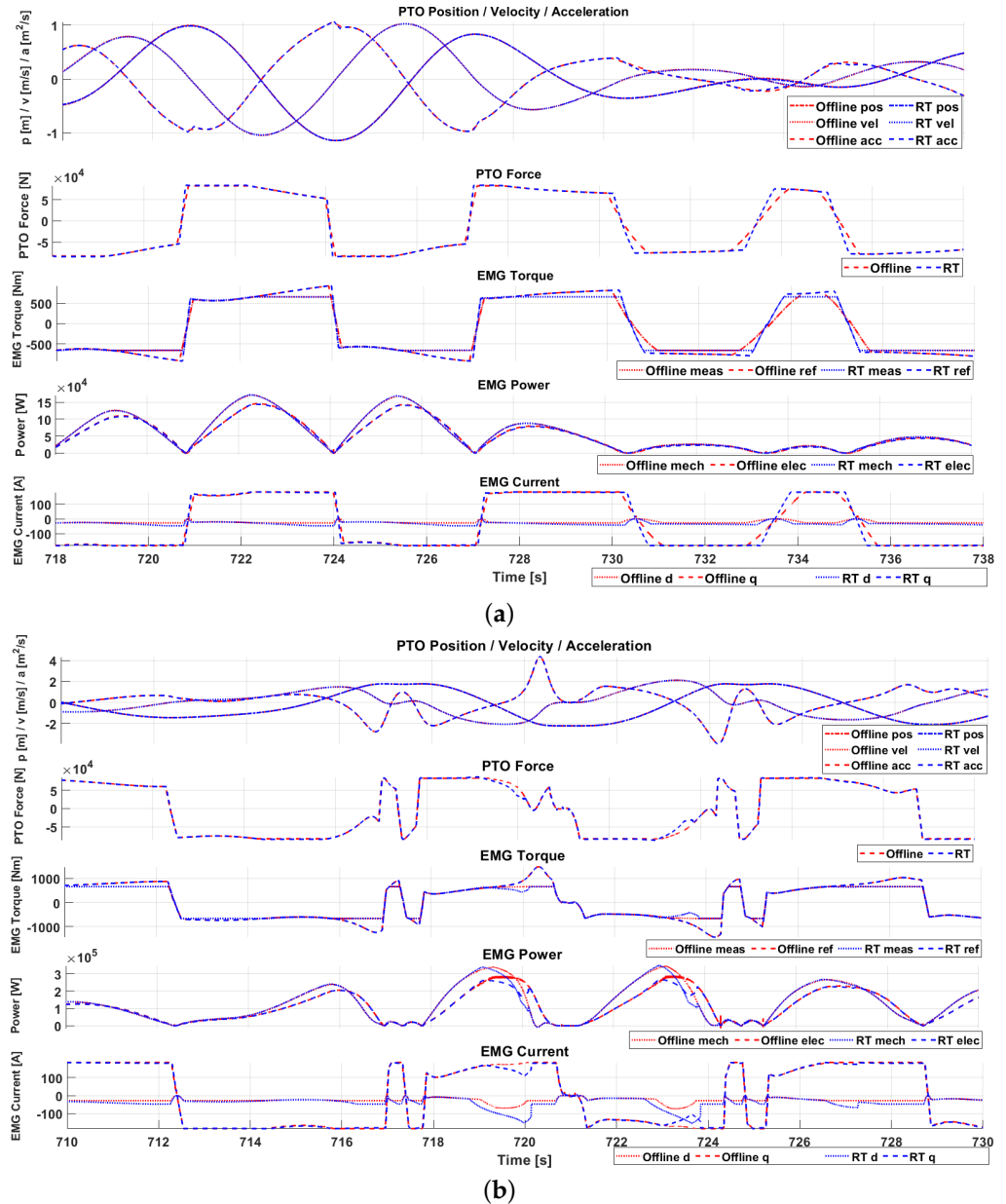

(a)

(b)

Figure 7. Visual comparison between offline and real−time models for two sea states: (**a**) $T_p = 7\,\text{s}$, $H_s = 2.25\,\text{m}$; (**b**) $T_p = 8\,\text{s}$, $H_s = 5.25\,\text{m}$.

6. Real-Time Model Used for Hardware-in-the-Loop Tests

In the last phase of the IMAGINE project, the HIL real-time model was updated in order to be interfaced with the real EMU and its power electronic converters. As indicated in Section 2, this configuration would allow us to test the unit up to its maximum operating limits, demonstrating the coherence with the input design data. This step was characterized by substantial changes in the model: firstly, the *Electric model* block was removed since it represents the PMSM, which is part of the EMU under test. The *CONTROLLER* block was also removed, since the respective algorithms were implemented on the programmable logic controller (PLC) of the EMU's power electronic converters. This option was preferred

to the one of having an hybrid control system (where part of the controller is within the real-time model and part within the PLC) to increase the performances of the system. In fact, while the real-time model required a minimum time step of 3 ms to be run, the PLC had a cycle time of 1 ms. In particular, the high-level controller implementing the PTO damping control strategy was computed by multiplying the damping factor by the synchronous speed of the EMU's electrical generator. Finally, the FW and MTPA algorithms were already implemented within the power and control system provided by the supplier.

Figure 8 represents the updated *SM_PLANT* of the RT model, which integrates the *wecSim model* block and the interface blocks from and to the rig. The *wecSim model* connects the real hardware system (e.g., EMU with its power and control system) to the simulated OWSC concept. This block was updated by removing the simulated interface with the EMU's input axis and by connecting it to the *EMU Ball-screw*, which sends the real output force measured from the load cell on the carriage of the test bench to the *wecSim model* block.
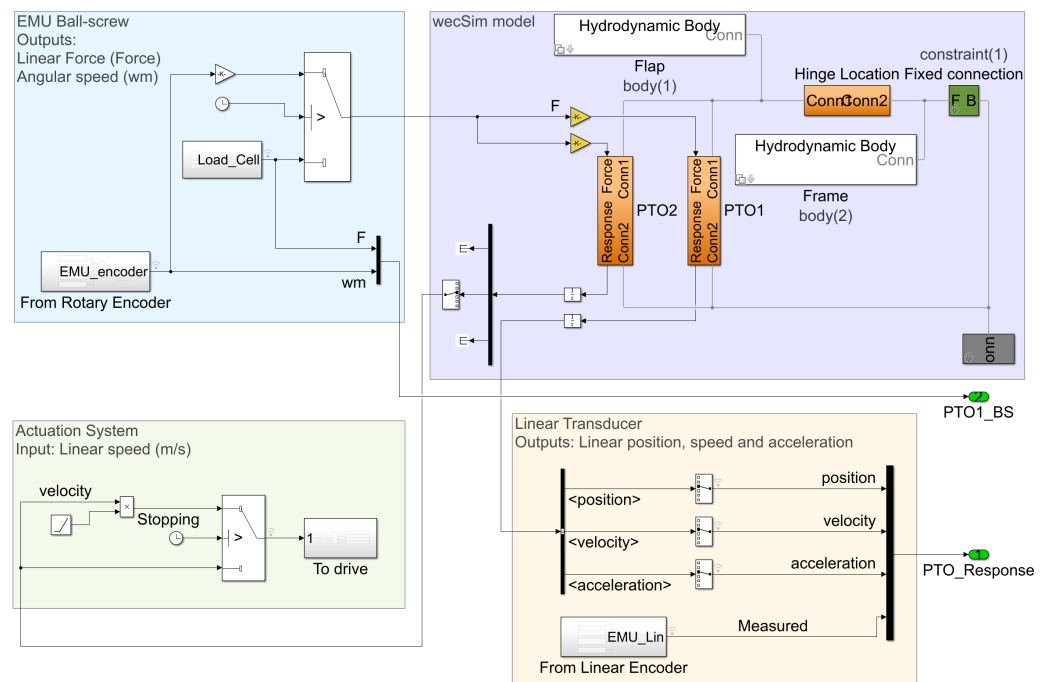

Figure 8. Matlab/Simulink Model for HIL tests including the WEC and interfaces with the test rig.

The *Actuation System* block uses the speed calculated from the *wecSim model* block and transfers it to the power and control system of the EMG to actuate the carriage. The feed-forward term accounting for the EMG's rotating inertia was implemented by increasing the motor shaft weight set on the software program of the power and control system. The other part of the feed-forward term (related to the EMG's frictions) was not implemented to reduce the computational burden of the PLC. Given the limited contribution that this term has on the overall force required at the axis, it was not expected to cause a difference in the test results.

Finally, the *Linear Transducer* block includes both simulated and measured linear kinematics, to allow for their comparison. In addition to the mentioned updates, the parameters within the controller of the actuation system had to be retuned to ensure the tests could be run smoothly. In particular, the fine-tuning of the speed derivative parameter was crucial to ensure a satisfactory performance.

7. Case Study with Real-Time Model Used for Hardware-in-the-Loop Tests

The results of the offline model and the real system were compared by running HIL tests with the EMG working as a actuator and the EMU working as a generator. The test

was executed while simulating the WEC in operational conditions for a total of 60 s with the sea state having the highest mean annual energy production ($T_p = 7$ s, $H_s = 2.25$ m). Figure 9 shows a visual comparison between the model and HIL test results for the same variables considered in Section 5. The figure highlights some differences between the two sets of results.
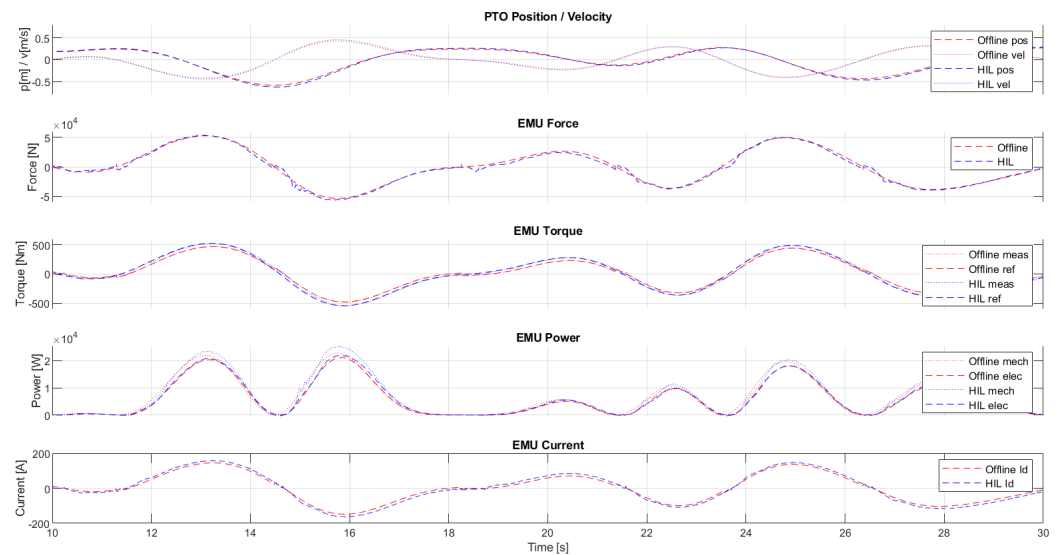

Figure 9. Comparison between offline model and HIL tests results for sea state with $T_p = 7$ s, $H_s = 2.25$ m.

In terms of kinematics, slight deviations between the respective positions (especially corresponding to the changes of direction) and speeds (corresponding to peak values) at the PTO input axis could be noticed. The input wave elevation being the same in the respective simulations (offline and real-time) and the speed output from the simulator to the actuation system being well aligned with the one measured by the encoder, the difference in terms of stroke and speed had to be related to a different behavior of the EMU. In particular, the parameters used for modeling the EMU in the offline model might not be the same as the ones of the real system.

When looking at the force profiles, a significant difference could be noticed corresponding to the stroke inversion, where the real EMU appeared to have a higher force with respect to the model. On the other hand, at maximum speed values the offline model and HIL tests reached similar values, with the EMU showing forces even beyond the ones foreseen from the offline model.

The torque did not behave like the force values: in the HIL test, the former was generally higher than the one simulated by the offline model. As a consequence of speed, torque, and (only for peaks) force having higher values in HIL tests, the input power, output power, and current profiles measured were beyond the values simulated in the offline model.

The discrepancies between simulated and real results could be corrected by updating the parameters describing the real behavior of the EMU within the offline model and rechecking the capacity of the power and control system to effectively apply the required control force.

In line with the case study described in Section 5, the NRMSE was used as metric to quantitatively compare the results; these are shown in Table 3. With respect to Table 2, the same reference parameters are shown, except for the acceleration, which was not measured during the tests. As seen in Figure 9, the correlation between the offline model and HIL tests was satisfactory. Lower values of NRMSE were, however, observed for the EMG's mechanical power and reference and measured torque, confirming an underestimation of these values by the offline model. The reason of this nonperfect correspondence was the incorrect estimation of the EMU's static and dynamic friction, whose coefficients had to be updated in the offline model to achieve more realistic results.

Table 3. NRMSE-based quantitative comparison between offline simulation and HIL real-time test.

Variable	$\mathbf{T_p = 7\,s}$ $\mathbf{H_s = 2.25\,m}$
PTO position	0.923
PTO velocity	0.935
PTO force	0.902
EMG's reference torque	*0.846*
EMG's measured torque	*0.856*
EMG's mechanical power	*0.845*
EMG's electrical power	0.928

8. Conclusions

This paper summarized the key findings related to the wave-to-wire models of an OWSC device connected to a PTO system (made of parallel EMUs) and to the HIL testing of the real EMU driven from a real-time simulator (implementing the same model, conveniently adapted).

First, an offline, detailed model of the overall system was created in the Matlab Simulink environment. The wave–flap interaction, its kinematics, and interface with the PTO were modeled through the use of the WEC-Sim toolbox. A block accounting for the mechanical and electrical aspects of the parallelized EMUs was included. A high-level controller and an electrical subsystem that included power converters and a dc link were modeled. The maximum torque per ampere and field-weakening techniques were also included in a low-level controller to adjust the electrical inputs to the PMSMs, according to the torque reference from the high-level controller.

Then, a real-time hardware-in-the-loop model was derived from the detailed model, to allow its execution on a RT platform, in view of the EMG's qualification tests. The simplification included the implementation of near-optimal MTPA and FW algorithms. A first comparison between the two models was presented considering the NRMSE as a quantitative metric. Values for the PTO position, velocity, and acceleration were above 0.96, which showed that the dynamics of the offline model were well represented by the RT model with execution times up to 10 times faster. However, differences in the force, reference, and output torques were present. These were mainly due to: (1) the discretization of control loops that introduced additional delays on the adjustment of the current; (2) the balance between i_d^*, i_q^* when the FW algorithm was applied. Both effects influenced the torque and force values exerted on the PMSM and ballscrew.

Finally, the real-time HIL model was adapted to allow the coupling with the real EMU under tests. The simplification included the removal of the electric model and controller block (substituted by real hardware and software). The interfaces between the simulation loop, the actuation system, and the EMU were realized by connecting the RT machine to the respective power electronic converters. The control strategies required for the actuator (feed-forward torque accounting for the mass) and generator (FW and MTPA) were implemented directly into the PLC's cyclic tasks. The overall simulation loop used the axial speed as the input of the plcs and the measured force at the carriage as the feedback to the simulator. A second comparison between the offline models and HIL test was presented; the results showed differences between the dynamics of the offline model and the ones of the tests, with the former mostly underestimating the latter.

The comparison between these three approaches is provided as a fundamental check to guarantee that the simulated environment is as similar as possible to the real space and hence to validate the product maturity albeit with a certain level of simplification.

References

1. European Commission. *Committing to Climate-Neutrality by 2050: Commission Proposes European Climate Law and Consults on the European Climate Pact*; EU Commission: Brussels, Belgium, 2020.
2. European Commission. *An EU Strategy to Harness the Potential of Offshore Renewable Energy for a Climate Neutral Future*; Communication COM(2020) 741 Final; European Commission: Brussels, Belgium, 2020.
3. Ocean Energy Forum. Ocean Energy Strategic Roadmap 2016: Building Ocean Energy for Europe. In Proceedings of the Ocean Energy Europe 2016 Conference & Exhibition: Brussels, Belgium, 8–9 November 2016.
4. TP Ocean. *Strategic Research Agenda for Ocean Energy*; Ocean Energy Europe: Brussels, Belgium, 2016.
5. ETIP Ocean. *Strategic Research and Innovation Agenda for Ocean Energy*; ETIP Ocean: Brussels, Belgium, 2020.
6. Carbon Trust. *Accelerating Marine Energy*; Technical Report CTC797; Carbon Trust: London, UK, 2011.
7. Castellini, L.; D'Andrea, M.; Borgarelli, N. Analysis and Design of a Reciprating Linear Generator for a PTO. In Proceedings of the 2014 International Symposium on Power Electronics, Electrical Drives, Automation and Motion, Ischia, Italy, 18–20 June 2014; pp. 1373–1379. [CrossRef]
8. Castellini, L.; D'Andrea, M.; Martini, M.; Alessandri, G.; Coiro, D.; De Luca, F.; Calise, G.; Troise, G.; Vogler, A. Experimental Tests on a Wave-to-Wire Pivoted System for Wave Energy Exploitation. In Proceedings of the 2017 6th International Conference on Clean Electrical Power (ICCEP), Santa Margherita Ligure, Italy, 27–29 June 2017; pp. 479–487. [CrossRef]
9. Cruz, J.; Atcheson, M.; Martins, T.; Castellini, L.; Martini, M. Preliminary Load Assessment: UMBRA's 250 kW EMG Power Take-Off. In Proceedings of the European Wave and Tidal Energy Conference, Naples, Italy, 1–6 September 2019; Volume 1.
10. Scriven, J.; Cruz, J.; Atcheson, M. Upscaling Wave Energy Converters: Size vs. Modularity. In Proceedings of the International Conference on Renewable Energies Offshore, Lisbon, Portugal, 12–15 October 2020.
11. Penalba, M.; Ringwood, J. A Review of Wave-to-Wire Models for Wave Energy Converters. *Energies* **2016**, *9*, 506. [CrossRef]
12. Zhou, X.; Zou, S.; Weaver, W.W.; Abdelkhalik, O. Assessment of Electrical Power Generation of Wave Energy Converters With Wave-to-Wire Modeling. *IEEE Trans. Sustain. Energy* **2022**, *13*, 1654–1665. [CrossRef]
13. Lin, Z.; Huang, X.; Xiao, X. Fast Model Predictive Control System for Wave Energy Converters With Wave Tank Tests. *IEEE Trans. Ind. Electron.* **2022**, 1–10. [CrossRef]
14. Penalba, M.; Ringwood, J.V. A high-fidelity wave-to-wire model for wave energy converters. *Renew. Energy* **2019**, *134*, 367–378. [CrossRef]
15. Henriques, J.; Gomes, R.; Gato, L.; Falcão, A.; Robles, E.; Ceballos, S. Testing and Control of a Power Take-off System for an Oscillating-Water-Column Wave Energy Converter. *Renew. Energy* **2016**, *85*, 714–724. [CrossRef]
16. Pedersen, H.; Hansen, R.; Hansen, A.; Andersen, T.; Bech, M. Design of Full Scale Wave Simulator for Testing Power Take Off Systems for Wave Energy Converters. *Int. J. Mar. Energy* **2016**, *13*, 130–156. [CrossRef]
17. Penalba, M.; Sell, N.; Hillis, A.; Ringwood, J. Validating a Wave-to-Wire Model for a Wave Energy Converter—Part I: The Hydraulic Transmission System. *Energies* **2017**, *10*, 977. [CrossRef]
18. Penalba, M.; Cortajarena, J.A.; Ringwood, J. Validating a Wave-to-Wire Model for a Wave Energy Converter—Part II: The Electrical System. *Energies* **2017**, *10*, 1002. [CrossRef]
19. Dang, T.D.; Phan, C.B.; Ahn, K.K. Modeling and Experimental Investigation on Performance of a Wave Energy Converter with Mechanical Power Take-Off. *Int. J. Precis. Eng. Manuf.-Green Tech.* **2019**, *6*, 751–768. [CrossRef]
20. Delmonte, N.; Robles, E.; Cova, P.; Giuliani, F.; Faÿ, F.X.; Lopez, J.; Ruol, P.; Martinelli, L. An Iterative Refining Approach to Design the Control of Wave Energy Converters with Numerical Modeling and Scaled HIL Testing. *Energies* **2020**, *13*, 2508. [CrossRef]

21. Castellini, L.; Gallorini, F.; Alessandri, G.; Alves, E.; Montoya, D.; Tedeschi, E. Performance Comparison of Offline and Real-Time Models of a Power Take-Off for Qualification Activities of Wave Energy Converters. In Proceedings of the 2021 16th International Conference on Ecological Vehicles and Renewable Energies (EVER), Monte-Carlo, Monaco, 5–7 May 2021; pp. 1–8. [CrossRef]

22. Yu, Y.H.; Ruehl, K.; Rij, J.V.; Tom, N.; Forbush, D.; Ogden, D.; Keester, A.; Leon, J. *WEC-Sim v4.2*; Zenodo: Geneva, Switzerland, 2020. [CrossRef]

23. Sjolte, J.; Sandvik, C.; Tedeschi, E.; Molinas, M. Exploring the Potential for Increased Production from the Wave Energy Converter Lifesaver by Reactive Control. *Energies* **2013**, *6*, 3706–3733. [CrossRef]

24. Li, M. Flux-Weakening Control for Permanent-Magnet Synchronous Motors Based on Z-Source Inverters. Master's Thesis, Marquette, Milwaukee, WI, USA, 2014.

25. Pan, C.T.; Liaw, J.H. A Robust Field-Weakening Control Strategy for Surface-Mounted Permanent-Magnet Motor Drives. *IEEE Trans. Energy Convers.* **2005**, *20*, 701–709. [CrossRef]

26. Lim, S. *Sensorless-FOC with Flux-Weakening and MTPA for IPMSM Motor Drives*; Technical Report SPRACF3; Texas Instruments; Dallas, TX, USA, 2018.

27. Lewis-Beck, C.; Lewis-Beck, M. *Applied Regression: An Introduction*; SAGE Publications, Inc.: Thousand Oaks, CA, USA, 2016. [CrossRef]

28. Franklin, G.F.; Powell, J.D.; Emami-Naeini, A. *Feedback Control of Dynamic Systems*, 6th ed.; Pearson: Upper Saddle River, NJ, USA, 2010.